

## Supplementary Information

### **CeO<sub>2</sub>/CuO/NiO hybrid nanostructures loaded on N-doped reduced graphene oxide nanosheets as an efficient electrocatalyst for water oxidation and non-enzymatic glucose detection**

Sahar Jafari<sup>a</sup>, Zohreh Shaghaghi\*

Coordination Chemistry Research Laboratory, Department of Chemistry, Faculty of Science,  
Azarbaijan Shahid Madani University, 5375171379, Tabriz, Iran

Email: shaghaghi@azaruniv.ac.ir, zsh024@gmail.com

#### List of Figures and Tables

**Table S1:** The onset potential and overpotential values for modified electrodes with nanomaterials.

**Fig. S1:** LSV curves of bare CPE and CPE in the presence of CeO<sub>2</sub>, CeO<sub>2</sub>/CuO, CeO<sub>2</sub>/NiO, and CeO<sub>2</sub>/CuO/NiO loaded on N-doped rGO in the potential range of 1.3-2.3 V vs. RHE and the scan rate of 50 mV s<sup>-1</sup> in a 25 mL of KOH solution (1M).

**Fig. S2:** FT-IR spectrum of CeO<sub>2</sub>/NiO nanostructures.

**Fig. S3:** PXRD pattern of CeO<sub>2</sub>/NiO nanostructures.

**Fig. S4:** FT-IR spectrum of CeO<sub>2</sub>@N-rGO.

**Fig. S5:** FT-IR spectrum of CeO<sub>2</sub>/CuO@N-rGO.

**Fig. S6:** FT-IR spectrum of CeO<sub>2</sub>/NiO@N-rGO.

**Fig. S7:** PXRD Pattern of CeO<sub>2</sub> and CeO<sub>2</sub>@N-rGO.

**Fig. S8:** PXRD Pattern of CeO<sub>2</sub>/CuO and CeO<sub>2</sub>/CuO@N-rGO.

**Fig. S9:** PXRD Pattern of CeO<sub>2</sub>/NiO@N-rGO.

## Synthesis and characterization of CeO<sub>2</sub>/NiO nanostructures

First, 25 ml of 0.02 M solution of Ce(NO<sub>3</sub>)<sub>3</sub>·6H<sub>2</sub>O and Ni(NO<sub>3</sub>)<sub>2</sub>·6H<sub>2</sub>O was prepared and transferred into a beaker. Then the pH was adjusted to 9 with 0.1 M K<sub>2</sub>CO<sub>3</sub> solution. The solution was stirred for 3 hours at room temperature. After that, the resulting precipitant was filtered and washed with DI water. Then, the solid was placed in an oven at 80° for 15 hours and calcinated at 700° for 4 hours in an electrical furnace.

FT-IR spectrum of CeO<sub>2</sub>/NiO nanostructures are given in Fig. S2. The absorption bands around 410 and 568 cm<sup>-1</sup> are attributed to the M-O stretching vibrations, while the absorption bands at wavenumbers of 1621 and 3420 cm<sup>-1</sup> are assigned to the bending and stretching vibrations of O-H bounds of water molecules, respectively which are adsorbed on the surface of nanoparticles.<sup>1-3</sup> Finally, the weak absorption peak at 1382 cm<sup>-1</sup> are assigned to the carbonate groups which are remained in the lattice of metal oxides. Fig. S3 shows the PXRD pattern of CeO<sub>2</sub>/NiO nanostructures. Distinct diffraction peaks at 2θ of 28.6°, 32.25°, 47.65°, 56.40°, 59.15°, 69.50°, 76.80°, and 79.20° correspond to (111), (200), (220), (311), (222), (400), (331), and (420) planes of cerium oxide, respectively, which is in good agreement with JCPDS 34-0394 and indicate the fluorite phase for CeO<sub>2</sub>.<sup>4</sup> In addition, characteristic peaks located at 2θ of 37.30°, 43.40°, and 63.00° are assigned to (111), (200), and (220) planes of nickel oxide crystal lattice (JCPDS 73-1523).<sup>5</sup> Comparing the PXRD pattern of pristine CeO<sub>2</sub> with CeO<sub>2</sub>/NiO shows that the prominent peaks of the CeO<sub>2</sub> are almost not shifted. However, some characteristic peaks of NiO are seen, indicating the presence of NiO in the cerium oxide network.

## **Synthesis and characterization of CeO<sub>2</sub>/N-rGO, CeO<sub>2</sub>/CuO@N-rGO, and CeO<sub>2</sub>/NiO@N-rGO nanocomposites**

0.05 g of pure CeO<sub>2</sub>, CeO<sub>2</sub>/NiO or CeO<sub>2</sub>/CuO was added to an aqueous solution of 0.05 g of graphene oxide in 50 ml of distilled water. Then, 0.05 mmol of urea was added to the reaction moiety, stirred for 10 min, and dispersed for 2 hrs in an ultrasonic bath. The obtained homogenous mixture was transferred into an autoclave and heated at 170 °C with a heating rate of 10 °C.min<sup>-1</sup> for 12 hrs. After cooling, the solid material was separated and washed with a 1:1 mixture of distilled water and ethanol and dried at 80 °C for 3 hrs.

The FT-IR Spectra of synthesized nanocomposites are shown in Figs. S4-S6. In the FT-IR spectra of nanocomposites, characteristic bands at the wavenumbers between 422 and 553 cm<sup>-1</sup> are related to the stretching vibrations of M-O bounds and the weak absorption band at 1381 cm<sup>-1</sup> is assigned to the carbonate groups remaining in the metal oxide network. A broad absorption band at around 3423-3448 cm<sup>-1</sup> corresponds to the stretching vibrations of hydroxyl groups of water molecules adsorbed on the metal oxide lattice, while the absorption band at about 1637-1640 cm<sup>-1</sup> is assigned to the bending vibrations of hydroxyl groups of water molecules. FT-IR spectra of CeO<sub>2</sub>/@N-rGO, CeO<sub>2</sub>/CuO@N-rGO, and CeO<sub>2</sub>/NiO@N-rGO shows both the absorption bands of CeO<sub>2</sub>, CeO<sub>2</sub>/CuO or CeO<sub>2</sub>/NiO and graphitic structure. As seen, the peaks related to the functional groups containing oxygen are significantly reduced in composites, indicating the presence of reduced graphene oxide. Finally, the observed weak bands at 1543-1563 cm<sup>-1</sup> and 1462 cm<sup>-1</sup> in the spectrum of nanocomposites are probably related to the C=N and C-N stretching vibrations.<sup>6-8</sup> In the PXRD pattern of CeO<sub>2</sub>/@N-rGO, the characteristic peaks corresponded to the CeO<sub>2</sub> are clearly seen at 2θ of 28.6° (111), 33.2° (200), 47.6° (220), 56.5°

(311), 59.2° (222), 69.6° (400), 76.8° (331), and 79.2°(420). In addition, the characteristic peak of rGO appears at about  $2\theta=23^\circ$ , which is assigned to the (002) plane.<sup>9,10</sup> As shown in Fig. S7, In the PXRD pattern of CeO<sub>2</sub>/@N-rGO, the diffraction peaks related to the cerium oxide almost remained unchanged compared to pure CeO<sub>2</sub>. For CeO<sub>2</sub>/CuO, distinct diffraction peaks at  $2\theta$  of 28.5°, 33.1°, 47.5°, 56.3°, 59.2°, 76.8°, and 79.2° correspond to (111), (200), (220), (311), (222), (331), and (420) planes of cerium oxide, respectively. In addition, characteristic peaks located at 35.8° (-111), 38.6° (111), 61.2° (-113), and 69.4° (-220) are attributed to the CuO crystal lattice.<sup>3</sup> The remaining weak peaks at  $2\theta$  of 25.4° and 41.4° are related to (002) and (100) planes of reduced graphene oxide. Comparing the PXRD pattern of CeO<sub>2</sub>/CuO and CeO<sub>2</sub>/CuO@N-rGO shows that the peaks of CeO<sub>2</sub> are almost not shifted. But, some characteristic peaks of copper oxide crystal lattice are seen, indicating the presence of CuO in the cerium oxide network (Fig. S8). Finally, the PXRD pattern of CeO<sub>2</sub>/NiO@N-rGO reveals diffraction peaks at  $2\theta$  of 28.7°, 33.2°, 47.6°, 56.4°, 59.2°, 66.9°, 76.7°, and 79.2° correspond to (111), (200), (220), (311), (222), (400), (331), and (420) planes of cerium oxide, respectively. Also, characteristic peaks located at  $2\theta$  of 37.2°, 43.5°, and 63.0° are related to (111), (200), and (220) planes of NiO. In addition, the characteristic peaks of rGO appears at  $2\theta$  of 23.2° and 40.4°, which is assigned to the (002) and (100) planes (Fig. S9). The appearance of some characteristic peaks of nickel oxide crystal lattice in the PXRD pattern indicates the presence of NiO in the cerium oxide network. Moreover, the absence of additional diffraction peaks implies the high crystalline nature of the obtained compounds.

## References:

1. O. Amadine, Y. Essamlali, A. Fihri, M. Larzek and M. Zahouily, *RSC advances*, 2017, **7**, 12586-12597.
2. Y. Guo, G. Wang, X. Yao and B. Liu, *Journal of Solid State Chemistry*, 2020, **292**, 121697.
3. Z. Shaghghi, S. Jafari and R. Mohammad-Rezaei, *Journal of Electroanalytical Chemistry*, 2022, **915**, 116369.
4. H. Lai, X. Zeng, T. Song, S. Yin, B. Long, A. Ali and G.-J. Deng, *Journal of Colloid and Interface Science*, 2022, **608**, 1792-1801.
5. S. Nagamuthu and K.-S. Ryu, *Scientific Reports*, 2019, **9**, 4864.
6. M. Suresh and A. Sivasamy, *Journal of Molecular Liquids*, 2020, **317**, 114112.
7. M. S. Lashkenari, S. Rezaei and J. Fallah, *Journal of Applied Electrochemistry*, 2021, **51**, 1267-1278.
8. A. Shanmugasundaram, N. D. Chinh, Y.-J. Jeong, T. F. Hou, D.-S. Kim, D. Kim, Y.-B. Kim and D.-W. Lee, *Journal of Materials Chemistry A*, 2019, **7**, 9263-9278.
9. S. Hassanpoor and F. Aghely, *Journal of the Iranian Chemical Society*, 2021, **18**, 993-1003.
10. L. Gai, C. Zhao, Y. Zhang, Z. Hu and Q. Shen, *Carbon Energy*, 2022, **4**, 142-154.

**Table S1:** The onset potential and overpotential values for modified electrodes with nanomaterials

Compound	Onset potential (V vs. RHE) at j of 10 mA cm <sup>-2</sup>	Overpotential (mV) at j of 10 mA cm <sup>-2</sup>
Bare CPE	2.025	795
CeO <sub>2</sub> /CPE	1.842	612
CeO <sub>2</sub> /CuO/CPE	1.820	590
CeO <sub>2</sub> /NiO/CPE	1.800	570
CeO <sub>2</sub> /CuO/NiO/CPE	1.760	530
GO/CPE	1.830	600
CeO <sub>2</sub> @N-rGO	1.720	490
CeO <sub>2</sub> /CuO@N-rGO	1.595	365
CeO <sub>2</sub> /NiO@N-rGO	1.580	350
CeO <sub>2</sub> /CuO/NiO@N-rGO	1.520	290

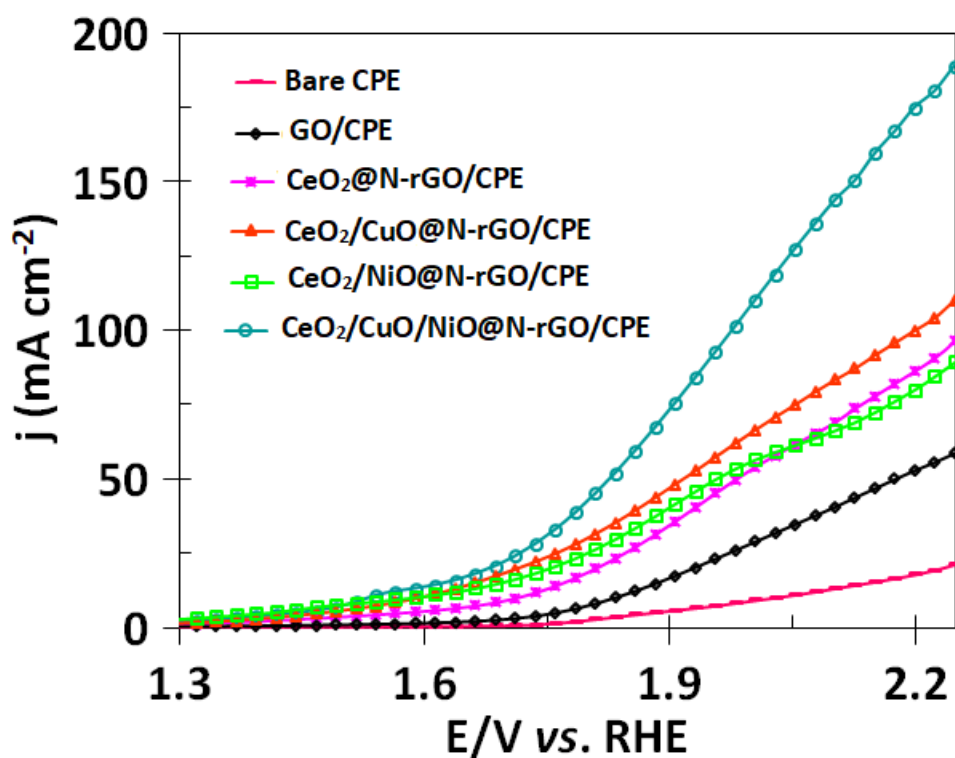


**Fig. S1:** LSV curves of bare CPE and CPE in the presence of CeO<sub>2</sub>, CeO<sub>2</sub>/CuO, CeO<sub>2</sub>/NiO, and CeO<sub>2</sub>/CuO/NiO loaded on N-doped rGO in the potential range of 1.3-2.3 V vs. RHE and the scan rate of 50 mV s<sup>-1</sup> in a 25 mL of KOH solution (1M).

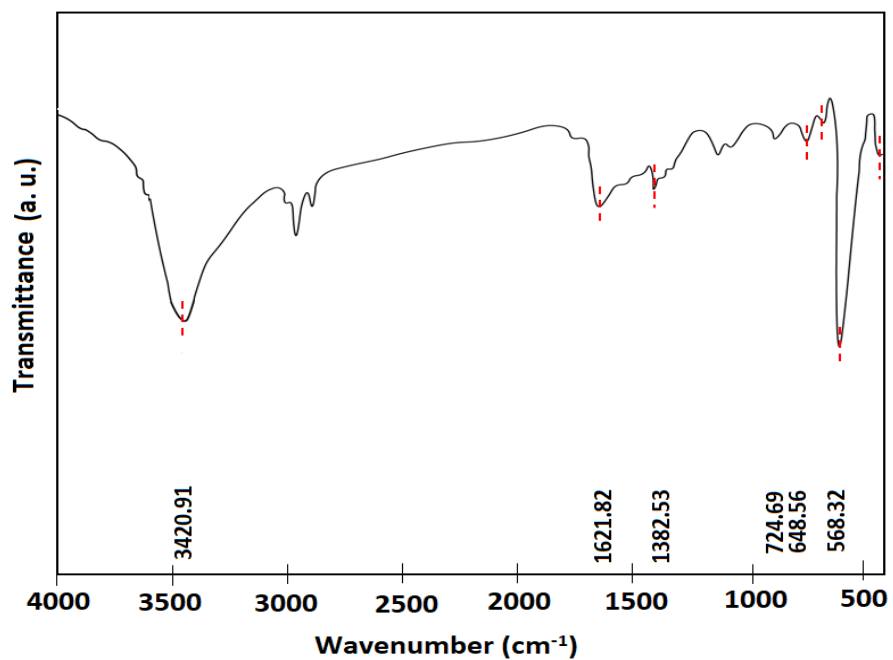


Fig. S2: FT-IR spectrum of CeO<sub>2</sub>/NiO nanostructures.

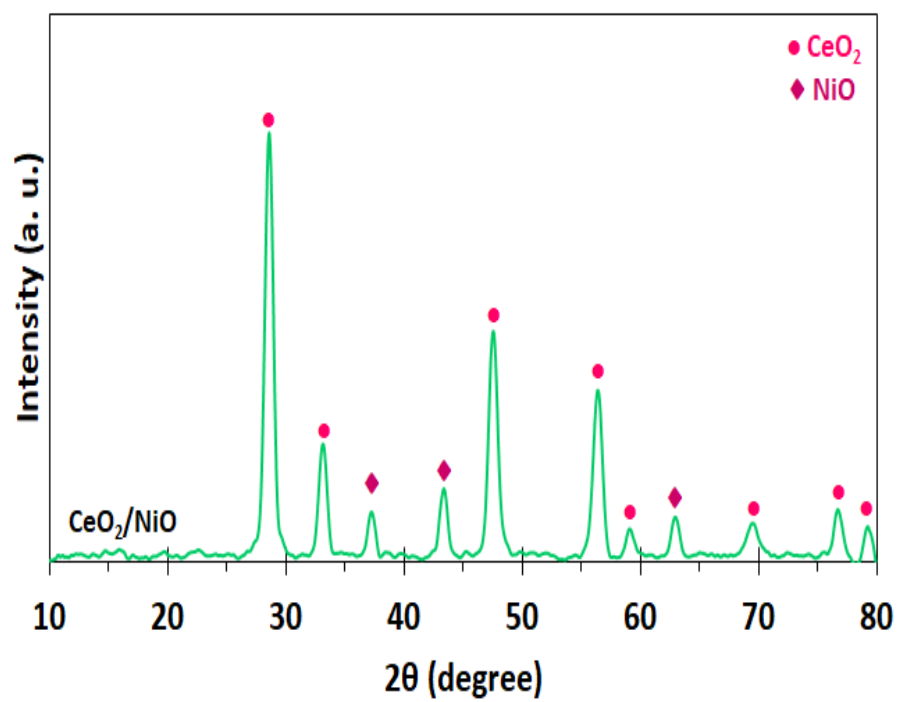


Fig. S3: PXRD pattern of CeO<sub>2</sub>/NiO nanostructures.

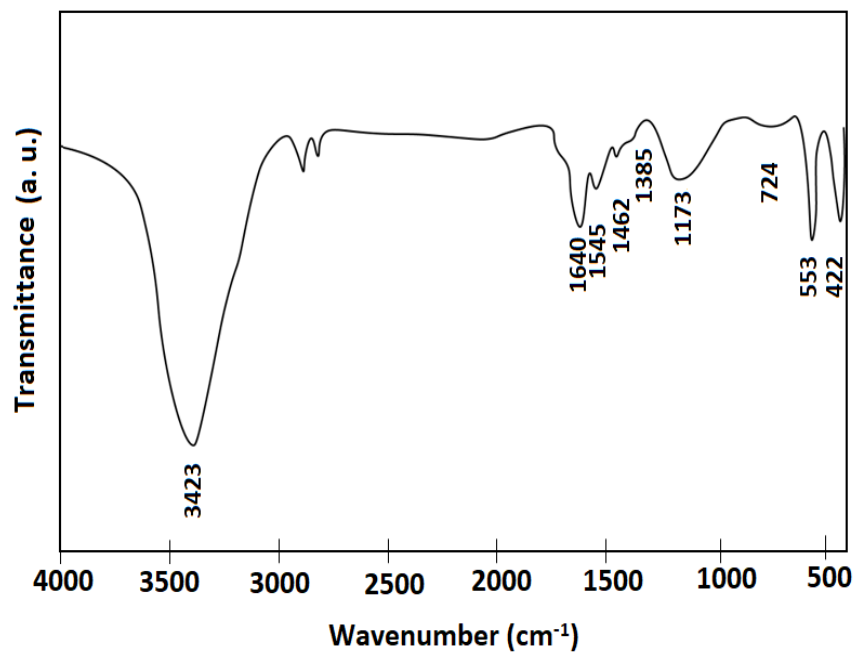


Fig. S4: FT-IR spectrum of CeO<sub>2</sub>@N-rGO.

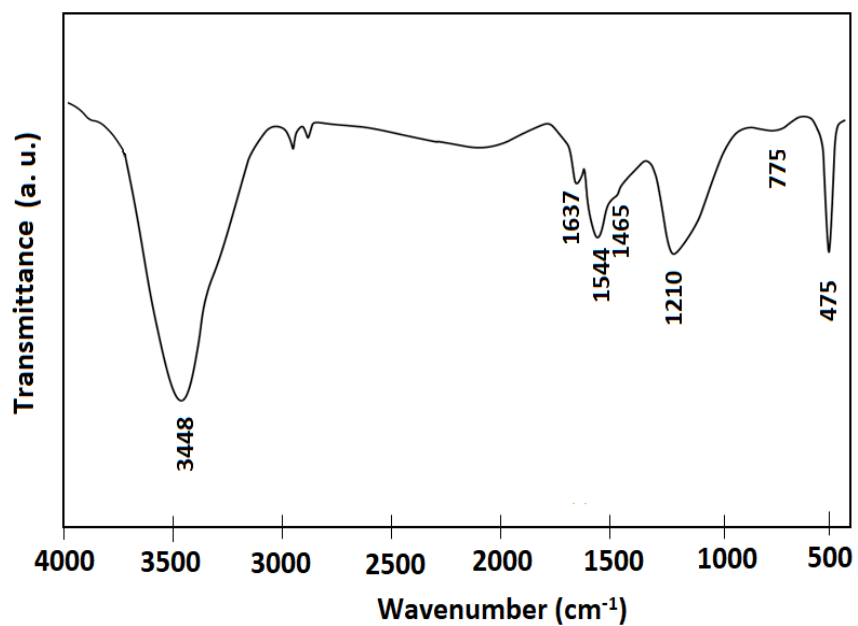


Fig. S5: FT-IR spectrum of CeO<sub>2</sub>/CuO@N-rGO.

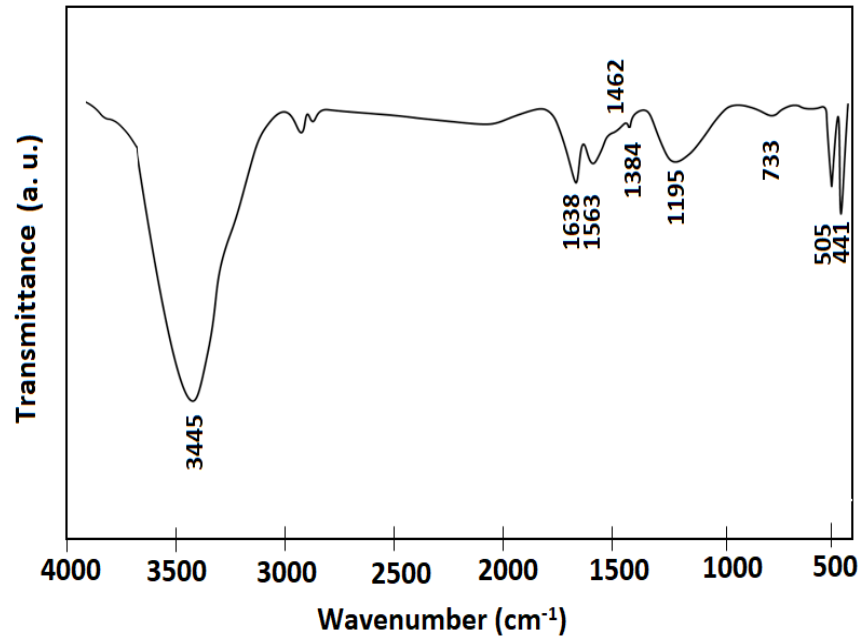


Fig. S6: FT-IR spectrum of CeO<sub>2</sub>/NiO@N-rGO.

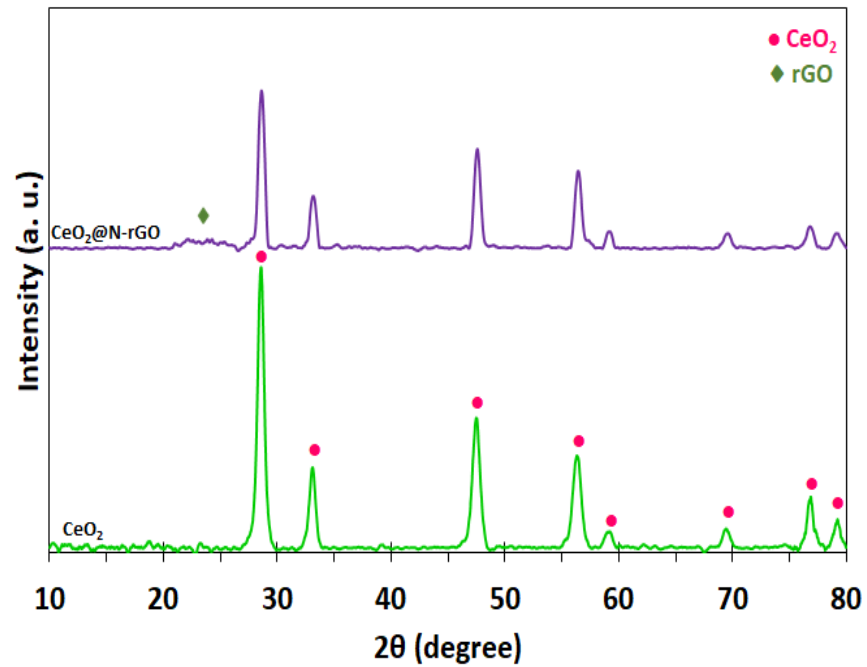


Fig. S7: PXRD Pattern of CeO<sub>2</sub> and CeO<sub>2</sub>@N-rGO.

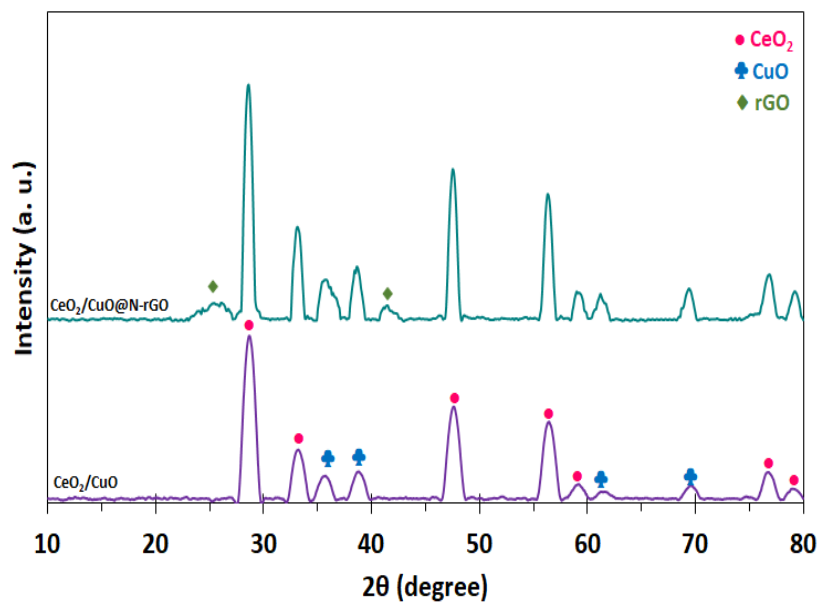


Fig. S8: PXRD Pattern of  $\text{CeO}_2/\text{CuO}$  and  $\text{CeO}_2/\text{CuO}@N\text{-rGO}$ .

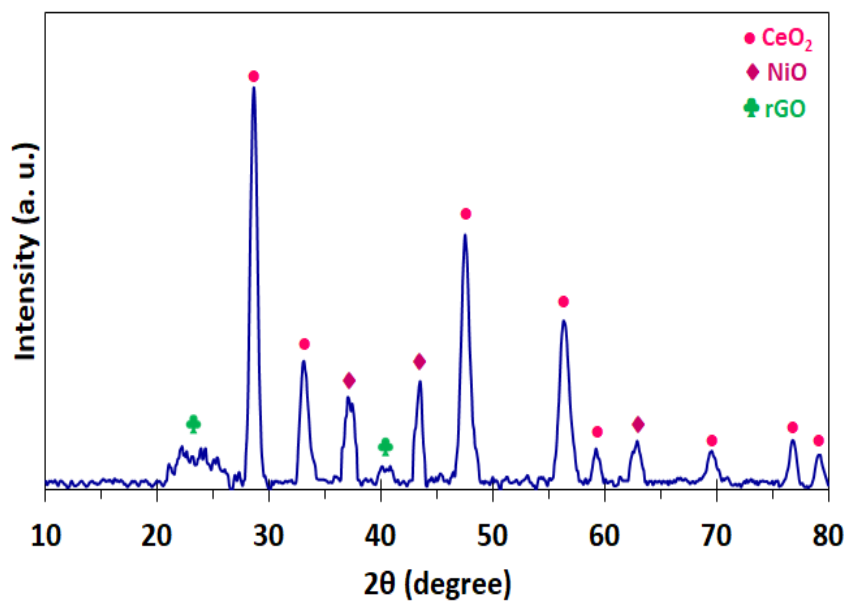


Fig. S9: PXRD Pattern of  $\text{CeO}_2/\text{NiO}@N\text{-rGO}$ .